Pre-combustion CO2 capture by transition metal ions embedded in phthalocyanine sheets

Kun Lü, Jian Zhou, Le Zhou, X. S. Chen, Siew Hwa Chan et al.

Citation: J. Chem. Phys. **136**, 234703 (2012); doi: 10.1063/1.4729471
View online: http://dx.doi.org/10.1063/1.4729471
View Table of Contents: http://jcp.aip.org/resource/1/JCPSA6/v136/i23
Published by the American Institute of Physics.

Pre-combustion CO_2 capture by transition metal ions embedded in phthalocyanine sheets

Kun Lü,[1] Jian Zhou,[2] Le Zhou,[2] X. S. Chen,[3] Siew Hwa Chan,[4] and Qiang Sun[1,2,a)]
[1]*Center for Applied Physics and Technology, Peking University, Beijing 100871, China*
[2]*Department of Materials Science and Engineering, College of Engineering, Peking University, Beijing 100871, China*
[3]*Shanghai Institute of Technical Physics, Chinese Academy of Science, Shanghai 200083, China*
[4]*Nanyang Technological University, 50 Nanyang Avenue, Singapore 639798, Singapore*

(Received 24 January 2012; accepted 29 May 2012; published online 20 June 2012)

Transition metal (TM) embedded two-dimensional phthalocyanine (Pc) sheets have been recently synthesized in experiments [M. Abel, S. Clair, O. Ourdjini, M. Mossoyan, and L. Porte, J. Am. Chem. Soc. **133**, 1203 (2010)], where the transition metal ions are uniformly distributed in porous structures, providing the possibility of capturing gas molecules. Using first principles and grand canonical Monte Carlo simulations, TMPc sheets (TM = Sc, Ti, and Fe) are studied for pre-combustion CO_2 capture by considering the adsorptions of H_2/CO_2 gas mixtures. It is found that ScPc sheet shows a good selectivity for CO_2, and the excess uptake capacity of single-component CO_2 on ScPc sheet at 298 K and 50 bar is found to be 2949 mg/g, larger than that of any other reported porous materials. Furthermore, electrostatic potential and natural bond orbital analyses are performed to reveal the underlying interaction mechanisms, showing that electrostatic interactions as well as the donation and back donation of electrons between the transition metal ions and the CO_2 molecules play a key role in the capture. © *2012 American Institute of Physics*. [http://dx.doi.org/10.1063/1.4729471]

INTRODUCTION

Nowadays with the rapid increase of the global population and the industrialization, the energy consumption is explosively growing. Carbon-based fossil fuels, which supply about 85% of the world's energy needs, are the main source of greenhouse gas (CO_2) contributing to the climate change. The severe weather perturbations and the global warming have stimulated scientists to find ways for reducing CO_2 emissions by 50% by 2050 in order to limit carbon concentration to 450 ppm.[1] Carbon capture and sequestration are considered as key options for this goal, where pre-combustion capture can be applied with fuels being gasified and converted to a mixture of mainly H_2 and CO_2 in a subsequent water-gas shift reaction. CO_2 can then be removed for disposal and the resultant H_2 could be used in fuel cells or in gas turbines. Further effort is needed to improve efficiency of CO_2 capture and to reduce operation cost. During the past few years, various CO_2 capture technologies have been explored.[2] An ideal material for pre-combustion capture of CO_2 should possess high selectivity and good adsorption capacity for CO_2. Recently, many porous materials for CO_2 capture have been synthesized, including covalent organic frameworks (COFs),[3,4] zeolitic imidazolate frameworks,[5,6] and metal organic frameworks (MOFs).[7–14] For example, Furukawa *et al.*[14] synthesized MOF-210 with Brunauer-Emmett-Teller and Langmuir surface areas of 4530 and 10 400 m^2/g, respectively. The CO_2 uptake of 2437 mg/g at ambient temperature and 50 bar exceeds those of any other porous materials.[14] However, the interaction between CO_2 and MOF-210 is still too weak to be suitable for pre-combustion CO_2 capture.

Recently, Abel *et al.*[15] have developed a synthesis technique where Fe-phthalocyanine (FePc) forms a periodic single layer sheet with regularly spaced Fe atoms. The synthesis procedure is flexible so that Fe atoms can be replaced by other metal atoms.[15–17] Due to its intrinsic high surface areas and polarity, together with the regularly and separately exposed transition metal (TM), the ScPc sheet has been identified as a promising hydrogen storage material.[18] The excellent performance of the ScPc sheet in hydrogen storage implies that it may also be a good candidate for CO_2 capture, which motivates us to investigate the CO_2 selectivity and capacity of TM (Sc, Ti, and Fe) embedded in Pc sheets in order to explore more efficient materials for trapping CO_2. In this work, based on first-principles density functional calculations and grand canonical Monte Carlo (GCMC) simulations, we have studied the CO_2 adsorption and CO_2/H_2 separation on TMPc (TM = Sc, Ti, and Fe) frameworks, and found that the ScPc framework has all the desirable features as a pre-combustion CO_2 capture material.

COMPUTATIONAL DETAILS

The geometric structures of two-dimensional (2D) ScPc, TiPc, and FePc have been optimized in our previous work.[18] We showed that the TiPc and FePc frameworks are both planar with the lattice constants of 10.7 Å, while in ScPc the Sc atoms tend to be located out of the plane by 0.67 Å because of the large radius of the Sc atom (Figure 1(a)). To calculate the CO_2 uptake of TMPc sheets at different pressure and ambient temperature, GCMC simulations are performed as

a)Author to whom correspondence should be addressed. Electronic mail: sunqiang@pku.edu.cn.

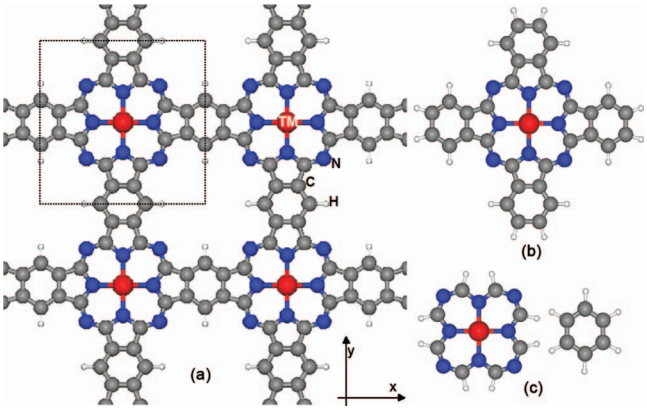

FIG. 1. (a) Geometry of TMPc sheet, (b) a cluster model used in geometry optimizations, and (c) cluster models for potential energy curve scanning.

implemented in the MUSIC code.[19] We used periodic boundary conditions with a vacuum space of 32 Å in the z direction between two nearest layers, and the supercell consists of 16 unit cells of the frameworks. CO_2 molecules were randomly inserted, translated, rotated, and deleted which allowed the number (N) of the total molecules and configurational energy (E) to fluctuate at constant temperature (T) and pressure (P). At any fixed T and P, 4×10^6 steps of GCMC simulations are used to guarantee the equilibrium followed by 6×10^6 steps to sample the thermodynamic properties. In this way, we can obtain absolute adsorption amount n_{abs} (the total number of CO_2 molecules present in one unit cell), while the excess adsorbed amount n_{ex} measured experimentally is determined by the following equation:

$$n_{ex} = n_{abs} - \rho(\mathrm{T}, \mathrm{P})\mathrm{V}_{\mathrm{free}}, \tag{1}$$

where ρ(T, P) is the molar density of the bulk gas phase calculated with the Peng-Robinson equation of state, and V_{free} is the total free volume within one unit cell that is not occupied by the framework atoms.

The force-field used in the GCMC calculations was fitted from the results of quantum mechanics calculations as implemented in the GAUSSIAN 09 package.[20] First, geometries of CO_2 adsorbed on different sites of TMPc were optimized by using a cluster model as shown in Figure 1(b), where the TMPc unit was frozen to keep the constrains in the 2D crystal lattice environment. The Perdew-Burke-Ernzerhof exchange-correlation functional[21] along with the LanL2DZ (Ref. 22) basis set was applied in optimization. In the favorite adsorbing configuration, we move the CO_2 molecule along the z axis to scan the potential energy curve. Such procedure can give accurate results and has been widely used.[23,24] To include nonlocal interactions between the CO_2 and the TMPc substrate, we used long range correlated hybrid functional WB97XD (Ref. 25) for exchange and correlation energy. The LanL2TZ+ (Ref. 22) (triple zeta basis designed for an effective core potential with diffuse d function) basis for Sc and the 6-311+g(d) basis for the other elements were used to the test of evaluating the influence of model size and structural variations on potential energy calculations. Then employing a higher level basis set def-TZVPPD (Ref. 26) (triple zeta valence basis set plus two sets of polarization and diffuse basis), and smaller cluster models (shown in Figure 1(c)), we scanned the potential energy curves of CO_2 adsorbed on the Sc(Ti, Fe)Pc sheet. We furthermore fit the nonbond potential energy U_{ij} between each two atoms using the combination of the Lennard-Jones (LJ) potential and the Coulomb potential

$$U_{ij}(r_{ij}) = 4\varepsilon\left[\left(\frac{\sigma}{r_{ij}}\right)^{12} - \left(\frac{\sigma}{r_{ij}}\right)^{6}\right] + \frac{q_i q_j}{r_{ij}}, \tag{2}$$

where ε represents the depth of the potential well, σ the finite distance at which the inter-particle potential is zero, q_i the atomic partial charge, and r_{ij} the distance between atoms i and j. Nonlinear least-squares fitting was performed with the initial value of the parameters taken from the universal force-field.[27] All parameters were independently varying during the fitting process. The force-field parameters describing the intermolecular interactions among CO_2 molecules were taken from the EPM2 model developed by Harris and Yung,[28] where CO_2 was modeled as a rigid linear molecule with three charged LJ sites located on each atom. The C–O bond length is 1.149 Å and partial point charges are $q_O = -0.3256e$ and $q_C = 0.6512e$. The LJ potential parameters are $\sigma_O = 3.033$ Å, $\epsilon_O/k_B = 80.507$ K for O atom and $\sigma_C = 2.757$ Å, $\epsilon_C/k_B = 28.129$ K for C atom. This potential model has been proven to give remarkable accuracy of the vapor-liquid phase equilibrium of CO_2.[28] While for the intermolecular interactions between CO_2 molecule and TMPc sheet, the partial charge of the atoms in TMPc sheet were obtained by using the ChelpG method[29] (i.e., the charge from electrostatic potentials (ESP) using a grid-based method). This method works by optimizing atomic charges in order to reproduce the electrostatic potential of the molecule. As such, the fitted atomic charges are particularly effective in the qualitative description of electrostatic interactions among interacting molecules. The LJ parameters were determined by fitting Eq. (2) to the potential energy curve. To get further insight into the interactions between the CO_2 molecule and TMPc sheet, we performed natural bond orbital (NBO) analysis[30] where the electronic wave function is interpreted in terms of a set of occupied Lewis orbitals and a set of unoccupied non-Lewis delocalized orbitals. For each donor NBO (i) and acceptor NBO (j), the stabilization energy $E(2)$ associated with charge transfer $i \rightarrow j$ is given by

$$E\,(2) = \Delta E_{ij} = q_i\left[\frac{F\,(i,\,j)^2}{\varepsilon_j - \varepsilon_i}\right], \tag{3}$$

where q_i is the donor orbital occupancy, and ε_i and ε_j are diagonal elements (orbital energies) and $F(i, j)$ is the off-diagonal NBO Fock matrix element.

RESULTS AND DISCUSSION

Figure 2 shows two optimized configurations of CO_2 adsorption on FePc. Configurations of CO_2 adsorbed on the Sc and Ti atoms in TMPc molecules are similar to the top configuration (b). The potential energy curve can be scanned along the z direction. To see the influence of model size and structural variations on potential energy calculations, detailed calculations were performed using different cluster models

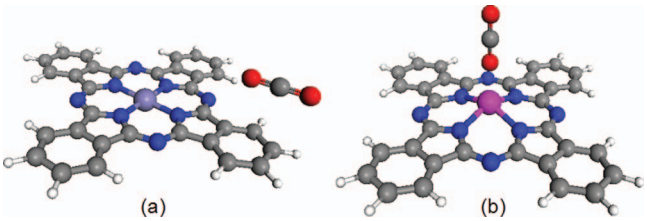

FIG. 2. One CO_2 molecule adsorbed with non-atop (a) and the atop (b) configurations.

shown in Figures 1(b) and 1(c) with unoptimized or partially optimized (the lateral carbon atoms were frozen) or fully optimized geometries, the results are shown in Figure 3. It can be seen that using unoptimized small cluster would slightly underestimate the adsorption energy. Considering the balance of the computational cost and precision, influences from the model size and small structural variations can be neglected in calculating potential energy. Figure 4 shows the potential energy curves calculated at high computational level. To see if basis sets superposition errors (BSSE) affect significantly the potential energy fitting, we did calculations with BSSE corrections, as shown in Fig. 4(b), which suggests that BSSE corrections make no improvement to the results, since the dispersion correction has been developed so that the small BSSE effects are absorbed into the empirical potential,[31] and hence being omitted in our calculations. Fitting the potential energy curve we obtain the LJ parameters (Figure 4), as listed in Table I. The nitrogen atoms are found to be in different

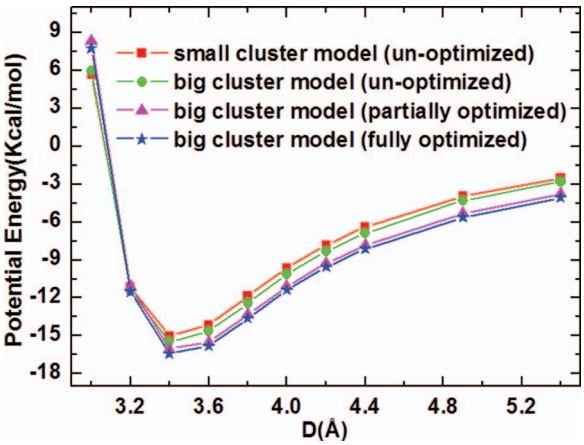

FIG. 3. Potential energy curves for different cluster models.

bonding environments: being bonded directly with TM atoms (labeled as N_TM), or being bonded only with C atoms (N′_C), accordingly different potential energy parameters are assigned to different nitrogen atoms for the sake of accuracy.

Using the fitted force-field parameters, GCMC simulations have been performed to predict the single-component CO_2 adsorption isotherms at ambient temperature. The results are given in Table II. It suggests that the CO_2 uptake capacity of ScPc sheet (2949 mg/g at 50 bar) has exceeded those of MOF-200 and MOF-210 having ultrahigh porosity and higher CO_2 uptake value than those of any other previously synthesized porous materials.[14] Besides, the TiPc sheet has a better

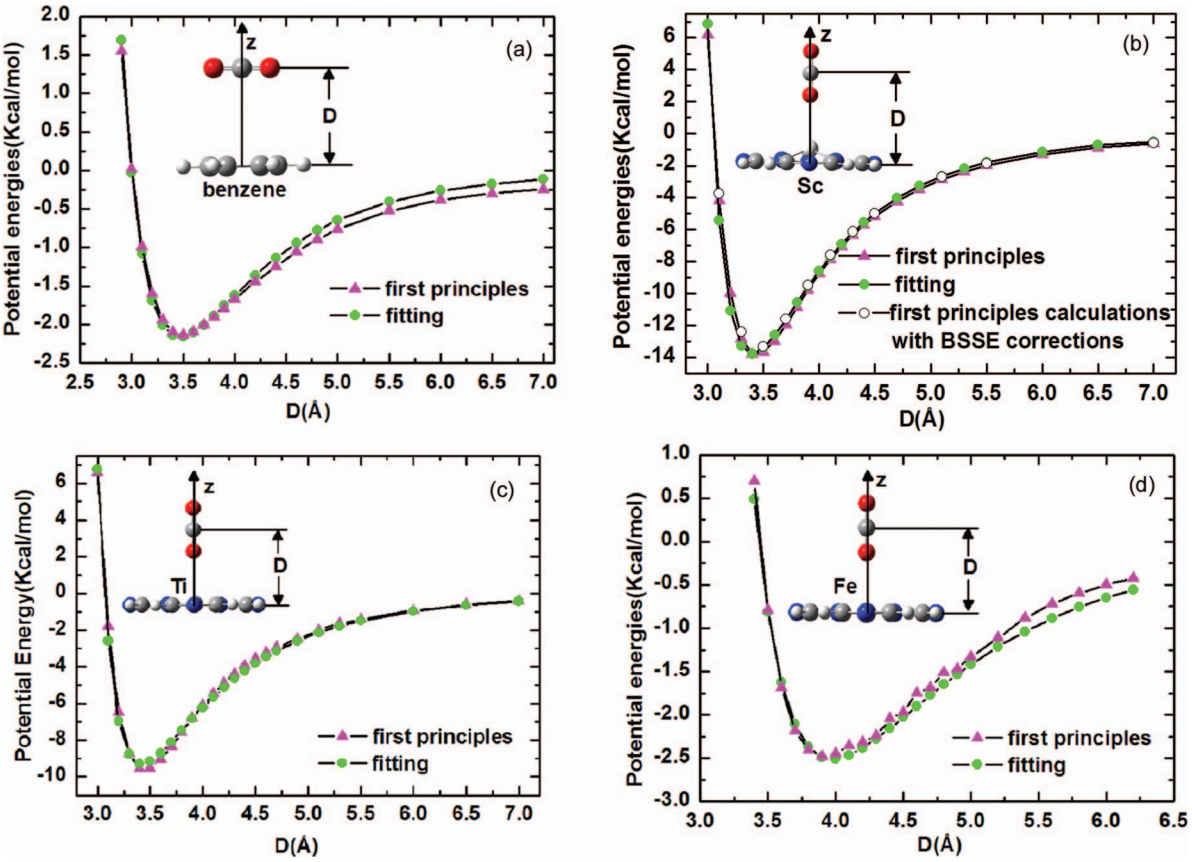

FIG. 4. Potential energy curves of CO_2 on small cluster model derived from first-principles calculations and classical force-field.

TABLE I. Fitted force-field parameters.

Term (C_CO_2–)	ε (kcal/mol)	σ (Å)	Term (O_CO_2–)	ε (kcal/mol)	σ (Å)
H_[a]	0.0649	3.12	H_	0.0890	3.77
C_[a]	0.1008	2.98	C_	0.1201	2.91
N′_C[b]	0.0648	3.37	N′_C	0.1785	3.88
N_Sc[c]	0.1578	3.87	N_Sc	0.1980	3.58
N_Ti	0.1581	3.75	N_Ti	0.0369	2.94
N_Fe	0.1634	2.51	N_Fe	0.0318	3.47
Sc	9.9863	2.90	Sc	2.1001	2.01
Ti	4.4956	3.02	Ti	1.4143	2.03
Fe	0.1669	3.81	Fe	0.1209	2.23

[a]H_ and C_ represent hydrogen and carbon atoms in TMPc sheets.
[b]N′ represents nitrogen atom bonded only to C atom.
[c]N represents nitrogen atom bonded to TM atoms directly.

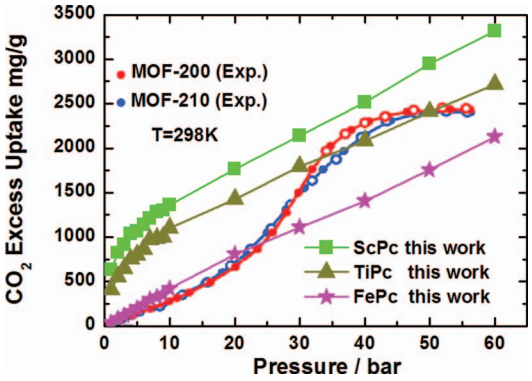

FIG. 5. Predicted CO_2 excess adsorption isotherms for different TMPc (TM = Sc, Ti, Fe) sheets at T = 298 K. The experimentally measured CO_2 isotherms of MOF-200 and MOF-210 at T = 298 K are also represented for comparison.

performance in CO_2 adsorption than most of the porous materials, while the FePc sheet adsorbs less CO_2 molecules as compared to ScPc and TiPc sheets. In Figure 5, we plot the simulated adsorption isotherms at T = 298 K. The experimentally measured CO_2 isotherms of MOF-200 and MOF-210 under the same condition[14] are also plotted for comparison. It can be seen that MOF-200 and MOF-210 show sigmoidal isotherms, which increase more slowly than those of TMPc sheets at low pressure (<15 bar), and then speed up and surpass the uptake of FePc and TiPc sheets under ~24 bar and ~35 bar, and finally saturated at ~50 bar. Whereas for the TMPc sheets, the isotherms are linear at moderate and high pressure and never reach saturation at a pressure up to 60 bar.

The CO_2 adsorption capacity is generally determined by the heat of adsorption (adsorption energy), surface area, and free volume of the porous material. Since the TMPc sheets are 2D materials, only surface area is meaningful. Below we show that the high CO_2 capacity of the TMPc sheet is due to the desirable adsorption energy.

We use the method of calculating the geometry surface area as explained in the work of Düren *et al.*[14,32] The results for ScPc, TiPc, and FePc sheets are 3600 m^2/g, 3584 m^2/g, and 3508 m^2/g, respectively, which are comparable to 3390 m^2/g of MOF-5,[14] but much less than 6400 m^2/g of MOF-200 (Ref. 14) and 5850 m^2/g of MOF-210.[14] According to Table II, the CO_2 uptakes of MOF-200 and MOF-210 at high pressure are nearly three times than that of MOF-5, owing to their ultrahigh porosity. Therefore, the relative smaller surface area cannot explain the high CO_2 adsorption capacities of TMPc sheets as compared to MOF-200 and MOF-210.

TABLE II. Comparison of high pressure CO_2 uptakes in different porous materials at T = 298 K.

Material	CO_2 uptake (mg g^{-1})	Material	CO_2 uptake (mg g^{-1})
Zeolites (Ref. 3)	220–350 (55 bar)	ScPc	2949 (50 bar)
COF-102 (Ref. 3)	1200 (55 bar)		3156 (55 bar)
COF-103 (Ref. 3)	1190 (55 bar)	TiPc	2412 (50 bar)
MOF-5 (Refs. 3 and 9)	864 (50 bar)		2569 (55 bar)
MOF-177 (Refs. 3 and 9)	1356 (50 bar)	FePc	1755 (50 bar)
MOF-200 (Ref. 14)	2437 (50 bar)		1960 (55 bar)
MOF-210 (Ref. 14)	2396 (50 bar)		

In order to better understand CO_2 capture by transition metal ions embedded in phthalocyanine sheets, we need to explore the relevant interacting mechanisms. Due to the linear symmetric structure, CO_2 molecule has no net charge and dipole moment but has a significant quadrupole moment induced by the large charge separation in the C=O bonds. According to the EPM2 model,[28] the quadrupole moment is calculated to be 4.1×10^{-26} esu, which is identical to the experimental value. The quadrupole shape of ESP of CO_2 shows a positive doughnut in the C plane and two negative lobes on both sides, as plotted in Figure 6(a). Because of its quadrupolar nature, CO_2 can act as a Lewis acid or a Lewis base:[33] CO_2 tends to interact with negative charges in a side-on geometry through a direct interaction with C,[34] whereas in the case of positive charges end-on adducts through one O are formed.[35] Figures 6(b)–6(d) show the ESP of ScPc, TiPc, and FePc molecules. The ESP around the TM atoms is always positive since the TM atoms donate their 4*s* electrons to the neighbor nitrogen atoms. The largest positive ESP can be seen near the Sc atoms which even covers the regions where negative charged nitrogen atoms are located. The ESP near the Ti atoms is weaker than that of the Sc atoms but still much stronger than that of Fe atoms. It can be concluded that the ScPc sheet has the strongest electrostatic interaction with the CO_2 molecule, followed by TiPc, and then FePc. This is consistent with the fact that the ScPc sheet performs best in adsorbing CO_2, followed by TiPc sheet and then FePc sheet.

It is well known that Sc and Ti are active TM atoms with low occupied 3*d* orbitals, which can bind H_2 through Kubas mechanism.[18,36] According to NBO analysis, we find a similar but stronger interaction between the TMPc and the CO_2 molecules as compared with the H_2-TMPc interaction. We identify that there are two main channels for electron transfer: one is from the Lewis NBOs of CO_2 to the low occupied hybrid orbitals of TM atoms, while the other is in an opposite direction. The strongest interactions for both channels of different complexes are extracted and shown in Figure 7. It can be seen that for the ScPc-CO_2 complex, the spin-up hybrid orbital of O with the component of $2s{:}2p_z = 1{:}0.54$,

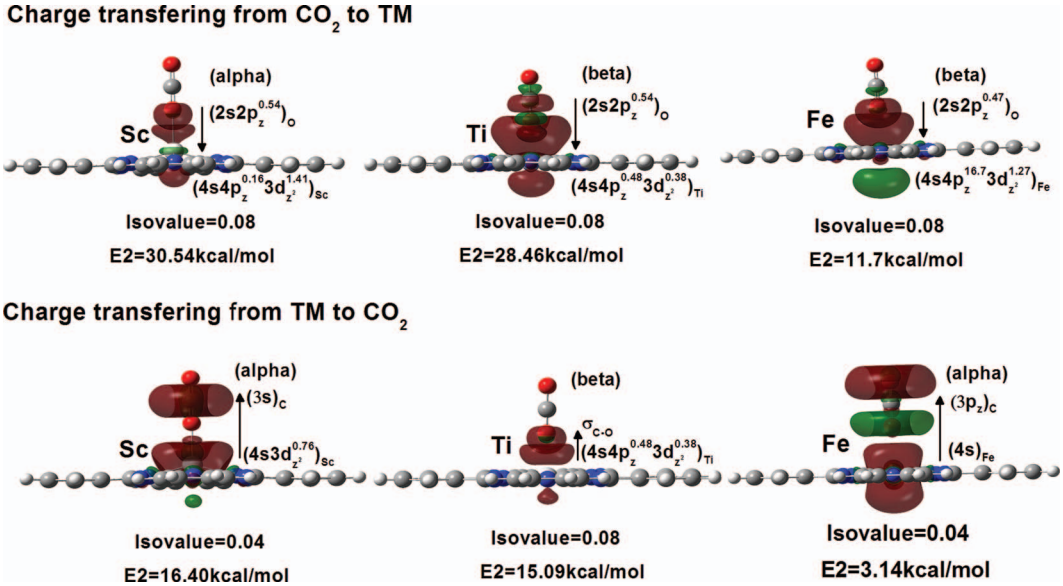

FIG. 6. Electrostatic potential map of (a) CO_2, (b) ScPc, (c) TiPc, and (d) FePc molecules.

overlaps with the hybrid orbital of Sc with the component of $4s : 4p_z : 3d_{z^2} = 1{:}0.16{:}1.41$. Electrons are donated from the former to the latter resulting in the stabilization energy $E(2)$ of 30.54 kcal/mol. Meanwhile, back donations take place between the hybrid orbital of Sc with the component of $4s : 3d_{z^2} = 1{:}0.76$ and the empty C-3*s*, lowing $E(2)$ by 16.40 kcal/mol. For the TiPc-CO_2 complex, the contribution to $E(2)$ by electron donation and back donation is 28.46 and 15.09 kcal/mol, respectively. It can be deduced from Figure 7 that the low occupied $3d_{z^2}$ orbital plays a dominant role in the charge donation channel for both ScPc-CO_2 and TiPc-CO_2 complexes. On the other hand, the d_{z^2} orbital of FePc-CO_2 complex is less involved in charge transfers, and the corresponding $E(2)$ for charge donation and back donation is only 11.7 kcal/mol and 3.14 kcal/mol, respectively. Besides the main charge transfer interactions shown in Figure 7, there are several other orbitals involved in minor donation and back donation which are not plotted. To see the whole picture, we summarize all the population changes in CO_2, and find electrons of 0.51162*e*, 44351*e*, and 0.0348*e* donated from the Lewis NBOs on CO_2 to the Sc, Ti, and Fe atoms, and 0.37526*e*, 0.33406*e*, and 0.01437*e* back donated from the Sc, Ti, and Fe atoms to the non-Lewis NBOs on CO_2, respectively, which indicates that ScPc has the most strong charge transfer interactions with CO_2.

According to the above analysis, we see that it is the strong electrostatic and charge transfer interactions between the ScPc sheet and CO_2 molecule that overcome the negative impact of relative smaller surface area of ScPc sheet and make it surpass MOF-200 and MOF-210 in adsorbing CO_2 at ambient environment. The sigmoidal shape of CO_2 adsorption isotherms in MOF-200 and MOF-210 can be interpreted by the rule proposed by Frost *et al.*[37] since the adsorptions of CO_2 and H_2 in MOFs are dominated by weak dissipation force. The situations are quite different in TMPc sheets. The uptake of CO_2 is found to be simply proportional to the density of CO_2, and thus proportional to the pressure as a result of quite strong interactions between CO_2 and TMPc sheets. This linear behavior is kept even under pressure of 60 bar. Similar linear CO_2 adsorption isotherm has also been found in Li-doped COF,[38] where positive charged Li ions introduce strong electrostatic interactions to CO_2 and COF.

Furthermore, the TMPc (TM = Sc, Ti, and Fe) sheets are tested for pre-combustion CO_2 capture via pressure swing adsorption (PSA), which is a widely used technology showing great potentials in CO_2 capture. Based on experimental findings that the mixtures in pre-combustion consist of ~40% CO_2 and 60% H_2 in a total pressure of 2.5–5 MPa,[39] we simulate the adsorption of the gas mixtures on TMPc sheets to

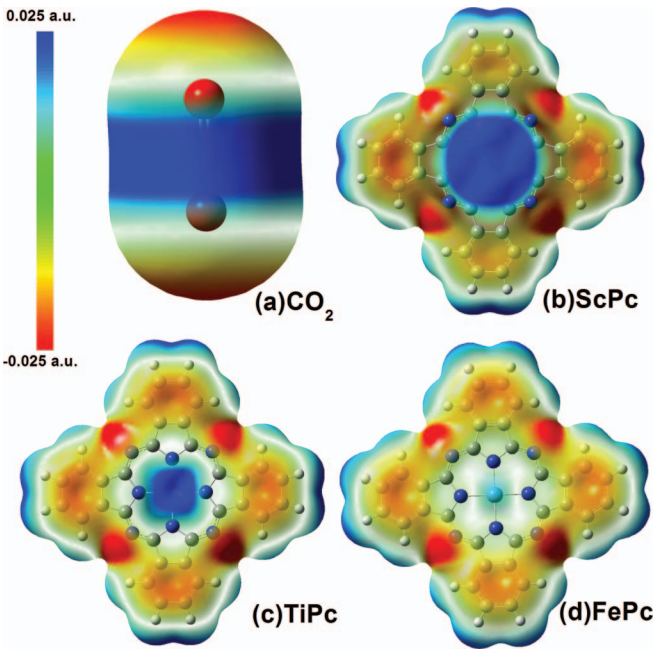

FIG. 7. Isosurface of main donor-acceptor interacting NBOs in different complexes.

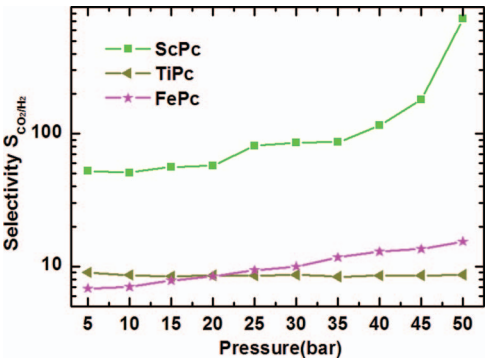

FIG. 8. CO_2/H_2 selectivities for a 60:40 H_2/CO_2 mixture at 313 K.

explore the selectivity for CO_2. We use the following definition of selectivity (or separation factor) for a binary gas adsorption[40]

$$S_{i,j} = \frac{x_i/y_i}{x_j/y_j},$$

where x_i and y_i are the mole fractions of the component-i in the adsorbed phase and in the gas phase at equilibrium, respectively. In our simulations, the force-field parameters of H_2 are taken from our previous paper.[18] Figure 8 shows the calculated selectivity for CO_2 over H_2 in 60:40 H_2/CO_2 gas mixture for different TMPc sheets. We can see that the ScPc sheet displays the highest selectivity, surpassing most adsorbents mentioned in Ref. 41 especially at high pressure. Further analysis reveals that at 50 bar (the partial pressure of H_2 is 30 bar), the TiPc and FePc sheets adsorb 1.9 and 0.4 more H_2 molecules per unit cell than that in ScPc sheet. The differences between the adsorption energies of CO_2-TM and H_2-TM are found to be $\Delta E_{Sc} = 0.28$ eV, $\Delta E_{Ti} = 0.032$ eV, and $\Delta E_{Fe} = 0.036$ eV, respectively, from which we can expect that the larger ΔE the better selectivity of CO_2 at higher pressure. This has been confirmed in our calculations as shown in Figure 8, suggesting that the ScPc sheet can be used for separation of CO_2 from H_2 better than most known adsorbent.

Another critical metric for evaluating adsorbents is working capacity defined as the difference between the capacity at the high intake pressure (50 bar) and at the lower purge pressure (1bar).[42] In PSA, CO_2 is adsorbed at syngas feed pressure (50 bar in our simulation model). Because of the high partial pressure of CO_2 in the mixture, the release of CO_2 can be achieved by reducing the pressure, which is energetically favorable and is more practical as compared with a temperature swing-based process. The results are shown in Figure 9. Comparing with the results of several MOFs and zeolites studied in Ref. 41, we find that the ScPc sheet outperforms the other adsorbents with a working capacity of 24.7 mol/kg at 50 bar. Therefore, the ScPc sheet is more efficient to capture CO_2 than the other materials.

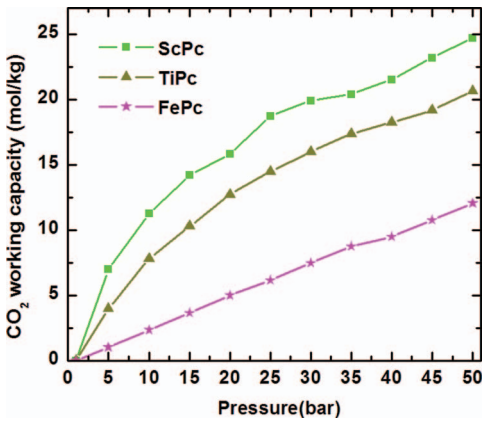

FIG. 9. CO_2 working capacities for 60:40 H_2/CO_2 mixture at 313 K.

TABLE III. Compositions of gases after water-gas shift reaction at 313 K and 30 bar in pre-combustion process, and the adsorption energies of the gas molecules on Sc sites calculated at the WB97XD/ LanL2TZ+ (for Sc)/6-311+g(d) (for the other elements) level with the big cluster model (Figure 1(b)).

Composition	Percentage (%)	Adsorption energy (eV)
H_2	61.5	0.229
CO_2	35.5	0.671
H_2O	0.2	1.499
CO	1.1	0.227
N_2	0.25	0.128
H_2S	1.1	0.980

Besides the two main gas components discussed above, product gases also contain some impurities. Table III summarizes our calculated adsorption energies for the typical gas compositions,[43] we can see that H_2S and H_2O molecules bind on Sc site more strongly than CO_2 molecule does. However in industry, H_2S (Refs. 39 and 44) and water vapor[45] are commonly removed prior to CO_2 capture for efficiency, the amounts of H_2S and H_2O molecules are so small that they are not sufficient to poison the adsorbent.

CONCLUSIONS

In summary, a synergistic study combining first-principles calculations and GCMC simulations is carried out to investigate the performance of TMPc (TM = Sc, Ti, and Fe) sheets for pre-combustion CO_2 capture. The following conclusions are obtained: (1) The CO_2 excess uptake capacity of the ScPc framework is 2949 mg/g at 298 K and 50 bar, which are higher than those of any reported porous materials; (2) Different from H_2, CO_2 has a significant quadrupole moment induced by the large charge separation in the C=O bonds, which induces strong electrostatic interactions. Detailed ESP and NBO analyses show that ScPc sheet has the strongest electrostatic interaction, electron donation and back donation with the CO_2 molecule, followed by TiPc sheet, and then FePc sheet; (3) For binary adsorption of 60:40 H_2/CO_2 mixture, the ScPc sheet shows ultrahigh CO_2/H_2 selectivity and CO_2 working capacity. The present study sheds light on better understanding of novel 2D porous nano-materials for CO_2 capture, which would stimulate further experimental effort in this direction.

ACKNOWLEDGMENTS

This work is partially supported by grants from the National Grand Fundamental Research 973 Program of China (2012CB921404), from the National Natural Science Foundation of China (NNSFC) (10990100, 20973010, 21173007), and from PKU CREATE project under the National Research Foundation (NRF), Singapore.

[1] D. Finon, Electricity Policy Research Group Working Paper **1035**, 1 (2010).
[2] D. Aaron and C. Tsouris, Sep. Sci. Technol. **40**, 321 (2005).
[3] H. Furukawa and O. M. Yaghi, J. Am. Chem. Soc. **131**, 8875 (2009).
[4] H. M. El-Kaderi, J. R. Hunt, J. L. Mendoza-Cortes, A. P. Cote, R. E. Taylor, M. O'Keeffe, and O. M. Yaghi, Science **316**, 268 (2007).
[5] R. Banerjee, A. Phan, B. Wang, C. Knobler, H. Furukawa, M. O'Keeffe, and O. M. Yaghi, Science **319**, 939 (2008).
[6] B. Wang, A. P. Côté, H. Furukawa, M. O'Keeffe, and O. M. Yaghi, Nature (London) **453**, 207 (2008).
[7] H. Li, M. Eddaoudi, T. L. Groy, and O. Yaghi, J. Am. Chem. Soc. **120**, 8571 (1998).
[8] H. Li, M. Eddaoudi, M. O'Keeffe, and O. M. Yaghi, Nature (London) **402**, 276 (1999).
[9] A. R. Millward and O. M. Yaghi, J. Am. Chem. Soc. **127**, 17998 (2005).
[10] P. K. Thallapally, J. Tian, M. Radha Kishan, C. A. Fernandez, S. J. Dalgarno, P. B. McGrail, J. E. Warren, and J. L. Atwood, J. Am. Chem. Soc. **130**, 16842 (2008).
[11] R. Babarao and J. Jiang, J. Am. Chem. Soc. **131**, 11417 (2009).
[12] A. Demessence, D. M. D'Alessandro, M. L. Foo, and J. R. Long, J. Am. Chem. Soc. **131**, 8784 (2009).
[13] D. Britt, H. Furukawa, B. Wang, T. G. Glover, and O. M. Yaghi, Proc. Natl. Acad. Sci. U.S.A. **106**, 20637 (2009).
[14] H. Furukawa, N. Ko, Y. B. Go, N. Aratani, S. B. Choi, E. Choi, A. O. Yazaydin, R. Q. Snurr, M. O'Keeffe, J. Kim, and O. M. Yaghi, Science **329**, 424 (2010).
[15] M. Abel, S. Clair, O. Ourdjini, M. Mossoyan, and L. Porte, J. Am. Chem. Soc. **133**, 1203 (2010).
[16] A. Sperl, J. Kröger, and R. Berndt, J. Am. Chem. Soc. **133**, 11007 (2011).
[17] J. Zhou and Q. Sun, J. Am. Chem. Soc. **133**, 15113 (2011).
[18] K. Lü, J. Zhou, L. Zhou, Q. Wang, Q. Sun, and P. Jena, Appl. Phys. Lett. **99**, 163104 (2011).
[19] A. Gupta, S. Chempath, M. Sanborn, L. Clark, and R. Snurr, Mol. Simul. **29**, 29 (2003).
[20] M. J. Frisch, G. W. Trucks, H. B. Schlegel *et al.*, GAUSSIAN 09, Revision B.01, Gaussian, Inc., Wallingford, CT, 2010.
[21] J. P. Perdew, K. Burke, and M. Ernzerhof, Phys. Rev. Lett. **77**, 3865 (1996).
[22] P. J. Hay and W. R. Wadt, J. Chem. Phys. **82**, 270 (1985).
[23] S. S. Han and W. A. Goddard, J. Am. Chem. Soc. **129**, 8422 (2007).
[24] D. Cao, J. Lan, W. Wang, and B. Smit, Angew. Chem., Int. Ed. **121**, 4824 (2009).
[25] J. D. Chai and M. Head-Gordon, Phys. Chem. Chem. Phys. **10**, 6615 (2008).
[26] D. Rappoport and F. Furche, J. Chem. Phys. **133**, 134105 (2010).
[27] A. Rappe, C. Casewit, K. Colwell, W. Goddard III, and W. Skiff, J. Am. Chem. Soc. **114**, 10024 (1992).
[28] J. G. Harris and K. H. Yung, J. Phys. Chem. **99**, 12021 (1995).
[29] C. M. Breneman and K. B. Wiberg, J. Comput. Chem. **11**, 361 (1990).
[30] A. E. Reed, L. A. Curtiss, and F. Weinhold, Chem. Rev. **88**, 899 (1988).
[31] S. Grimme, J. Comput. Chem. **27**, 1787 (2006).
[32] T. Düren, F. Millange, G. Férey, K. S. Walton, and R. Q. Snurr, J. Phys. Chem. C **111**, 15350 (2007).
[33] P. Raveendran, Y. Ikushima, and S. L. Wallen, Acc. Chem. Res. **38**, 478 (2005).
[34] J. M. Weber and H. Schneider, J. Chem. Phys. **120**, 10056 (2004).
[35] B. Bonelli, B. Civalleri, B. Fubini, P. Ugliengo, C. O. Areán, and E. Garrone, J. Phys. Chem. B **104**, 10978 (2000).
[36] J. Kubas Gregory, Acc. Chem. Res. **21**, 120 (1988).
[37] H. Frost, T. Düren, and R. Q. Snurr, J. Phys. Chem. B **110**, 9565 (2006).
[38] J. Lan, D. Cao, W. Wang, and B. Smit, ACS Nano **4**, 4225 (2010).
[39] P. Linga, R. Kumar, and P. Englezos, J. Hazard. Mater. **149**, 625 (2007).
[40] D. M. Ruthven, *Principles of Adsorption and Adsorption Processes* (Wiley-Interscience, 1984).
[41] Z. R. Herm, J. A. Swisher, B. Smit, R. Krishna, and J. R. Long, J. Am. Chem. Soc. **133**, 5664 (2011).
[42] M. T. Ho, G. W. Allinson, and D. E. Wiley, Ind. Eng. Chem. Res. **47**, 4883 (2008).
[43] D. M. D'Alessandro, B. Smit, and J. R. Long, Angew. Chem., Int. Ed. **49**, 6058 (2010).
[44] C. C. Cormos, F. Starr, E. Tzimas, and S. Peteves, Int. J. Hydrogen Energy **33**, 1286 (2008).
[45] G. Li, P. Xiao, P. A. Webley, J. Zhang, and R. Singh, Energy Procedia **1**, 1123 (2009).